Asian Journal of Pharmaceutical Sciences 17 (2022) 87–101

Available online at www.sciencedirect.com

ScienceDirect

journal homepage: www.elsevier.com/locate/AJPS

Original Research Paper

# Sodium alginate and naloxone loaded macrophage-derived nanovesicles for the treatment of spinal cord injury

*Xiaoyao Liu*[a], *Xue Jiang*[a], *Qi Yu*[a], *Wenwen Shen*[a], *He Tian*[c], *Xifan Mei*[b,*], *Chao Wu*[a,*]

[a] *Pharmacy School, Jinzhou Medical University, Jinzhou 121001, China*
[b] *Department of Orthopedics, The First Affiliated Hospital of Jinzhou Medical University, Jinzhou 121004, China*
[c] *Department of Histology and Embryology, Jinzhou Medical University, Jinzhou 121001, China*

ARTICLE INFO

*Article history:*
Received 24 July 2021
Revised 6 November 2021
Accepted 9 November 2021
Available online 14 November 2021

*Keywords:*
Naloxone
Sodium alginate
Spinal cord injury
Macrophage membrane
Inflammation
Neuroprotection

ABSTRACT

Spinal cord injury (SCI) causes $Ca^{2+}$ overload, which can lead to inflammation and neuronal apoptosis. In this study, we prepared a nanovesicle derived from macrophage membrane (MVs), which encapsulated sodium alginate (SA) and naloxone (NAL) to inhibit inflammation and protect neurons by reducing the free $Ca^{2+}$concentration at the SCI site. Based on the transmission electron microscopy (TEM) image, the encapsulated sample (NAL–SA–MVs) had a particle size of approximately 134 ± 11 nm and exhibited a sustained release effect. The encapsulation rate of NAL and SA was 82.07% ± 3.27% and 72.13% ± 2.61% in NAL–SA–MVs, respectively. Targeting tests showed that the NAL–SA–MVs could accumulate in large quantities and enhance the concentration of SA and NAL at the lesion sites. *In vivo* and *in vitro* studies indicated that the NAL–SA–MVs could decrease the concentration of free $Ca^{2+}$, which should further alleviate the inflammatory response and neuronal apoptosis. Anti-inflammation results demonstrated that the NAL–SA–MVs could reduce the pro-inflammation factors (iNOS, TNF-$\alpha$, IL-1$\beta$, IL-6) and increase the expression of anti-inflammation factors (IL-10) at the cell and animal level. Concurrently, fluorescence, flow cytometry and western blot characterization showed that the apoptotic condition of the neurons was significantly inhibited. In addition, the motor function of C57 mice were significantly improved after NAL–SA–MVs treatment. In conclusion, it is suggested that the NAL–SA–MVs has tremendous potential in the treatment of SCI.



* Corresponding author.
*E-mail addresses:* meixifan@jzmu.edu.cn (X.F. Mei), wuchao@jzmu.edu.cn (C. Wu).
Peer review under responsibility of Shenyang Pharmaceutical University.

https://doi.org/10.1016/j.ajps.2021.11.001

## 1. Introduction

Traffic accidents, falls from heights, or other causes lead to approximately one million new spinal cord injury (SCI) cases worldwide each year. SCI is a serious and traumatic disease [1], which poses a heavy burden on the society and individuals [2,3]. It can be broadly divided into two phases: primary and secondary injury [4]. Primary injury is severe damage to the spinal cord tissue, causing damage and even death of microglia and motor neuron cells of spinal cord anterior horn. Secondary injury is caused by hypoxia and intracellular $Ca^{2+}$ overload, resulting in hemorrhage and edema at the site of injury, and it can produce numerous inflammatory mediators and result in neuronal damage. Many studies have shown that secondary injury is an important stage in the treatment of SCI [5–7]. Currently, the treatment mainly focuses on reducing inflammation and providing neuroprotection [8,9]. There are many nanocarriers that played an important role by delivering effective drugs to the site of injury, such as nanogel [10], exosomes [11], liposomes [12], nanoparticles [13], nano-micelle [14], etc. However, owing to the low efficiency of some drugs in crossing the blood-brain/blood-spinal cord barrier (BBB/BSCB), it cannot exert adequate therapeutic effect [15]. Therefore, it is very significant to find a suitable drug transporter to improve drug targeting.

In recent years, several researchers have developed a significant interest in cell membrane-derived transporters. Different sources of cell membrane impart drug transporters with varied functions. For example, neutrophil membrane-derived nanovesicles have inflammatory orientation functions [16], erythrocyte membrane-derived biomimetic engineered delivery systems possess high immune escape ability [17], and platelet membrane-derived biomimetic nanobubble can tightly bind to injured blood vessels [18]. In addition to the above cell membranes, macrophage membranes are commonly used owing to the advantages of low immunogenicity, good biocompatibility, good biodegradability, long circulation, tendency to inflammation, and easy crossing of the blood–brain barrier. Our previous research demonstrated that macrophage-derived nanovesicles encapsulated with nerve growth factor (NGF) can play a neuroprotective role and promote the recovery of motor function after SCI [19]. Therefore, macrophage membranes-derived drug delivery carriers have high potential anti-inflammatory, neuroprotective and motor recovery applications after SCI.

After SCI, extracellular $Ca^{2+}$ flow entry and intracellular $Ca^{2+}$ release also increase significantly. However, owing to the lack of adenosine triphosphate (ATP), the excess intracellular $Ca^{2+}$ cannot be pumped out normally, which eventually increases the $Ca^{2+}$ level at the SCI site [20–22]. Sodium alginate (SA) is a natural polysaccharide extracted from brown algae and has the safety requirements for pharmaceutical excipients [23]. It can chelate with $Ca^{2+}$ rapidly and irreversibly to form a calcium alginate gel [24,25]. This process can significantly reduce the concentration of free $Ca^{2+}$ at the site of injury, ultimately reducing the inflammation and nerve damage.

Naloxone (NAL) is an opioid receptor antagonist with no intrinsic activity. However, it can competitively antagonize various types of opioid receptors with a strong affinity for μ receptors [26]. It is frequently used in the differential diagnosis of opioid overdose-induced respiratory depression, coma, and opioid addiction. Previous studies showed that NAL has a key therapeutic role in spinal cord injury [27–30]. It can reduce $Ca^{2+}$ concentration, inhibit the activation of microglia and the release of inflammatory cytokines as well as play a neuroprotective role [31]. However, NAL has a short half-life and poor bioavailability, which makes it difficult to exert its full pharmacological effects on SCI sites. To overcome these drawbacks, we encapsulated SA and NAL in macrophage-derived membranes to form nanovesicles. This approach can not only target SA and NAL to the injury site for synergizing to reduce the concentration of free $Ca^{2+}$, but also significantly inhibit the release of inflammatory factors and the injury of neurons. These properties are of significance in the treatment of SCI and provide a new concept for its clinical treatment.

## 2. Materials and methods

### 2.1. Materials

Naloxone was purchased from Taizhou Hongyao Chemical Co., Ltd. Naltrexone and phloroglucinol were supplied by Aladdin. The dialysis bags, FITC, fura-2AM fluorescent probe, nissl staining solution, hematoxylin eosin (HE) staining kit and BCA protein concentration determination kit were ordred from Beyotime Biotechnology. LPS, Fetal bovine serum (FBS), DMEM, penicillin-streptomycin (PS) and trypsin-EDTA (0.25%) were purchased from Gibco Company. Protein lysate (RIPA), phenylmethanesulfonyl fluoride (PMSF) and 4′,6-diamidino-2-phenylindole (DAPI) were bought from Beijing Solarbio Science & Technology Co., Ltd. Anti-CD11b, anti-F4/80, anti-iNOS, anti-TNF-$\alpha$, anti-IL-1$\beta$, anti-IL-6, anti-IL-10, anti-Bax, anti-caspase 3, anti-bcl-2, anti-$\beta$-tubulin, anti-GAPDH, anti-$\beta$-actin were supplied by Abcam.

### 2.2. Cell culture

$BV_2$ and VSC4.1 cells were obtained from the Chinese Academy of Sciences Cell Bank and grown in a humidifying atmosphere with 5% $CO_2$ at 37 °C constant temperature. The medium was Dulbecco's modified eagle medium (DMEM) (Gibco, Grand Island, NY, USA) containing 10% fetal bovine serum, 1% penicillin, and 1% streptomycin. The cells were digested with 0.25% trypsin during cell subculture.

### 2.3. Animals and the SCI model

C57BL/6J mice (10–12 weeks, 18–25 g, half male and half female) were bred at the SPF Experimental Animal Center of Jinzhou Medical University, with five mice in each cage. The temperature and humidity were appropriate, the light and shade were alternated for 12 h, and the mice had sufficient food and water. The animal experiment scheme was approved by the Experimental Animal Ethics Committee of Jinzhou Medical University.

The SCI model was established by Allen's method [32,33]. The mice were first anesthetized by injecting 1% pentobarbital sodium and placed in a prone position, and then the back hair of T9/T10 was removed. We applied povidone-iodine for disinfection, incised the skin and subcutaneous tissue, and selected the T9 spine to lift the vertebral plate for exposing the spinal cord completely. Subsequently, an impactor device (12.5 g) was used to cause moderate contusion of the spinal cord by dropping it at 1 cm, and the mice were successfully molded when they showed hind limb spasm. The sham group simply lifted the vertebral plates and did not deliver a blow to the spinal cord. Then the muscle and the skin were sutured together layer-wise, coated with povidone-iodine to prevent the mice from tearing each other, and place in cages. Penicillin was administered for 7 d to prevent infection. The mice were randomly divided into 5 groups including sham group, SCI group, NAL, SA–MVs and NAL–SA–MVs group. And the isotonic saline or corresponding drugs were injected by tail vein once a day and lasted for 7 d.

### 2.4. *Extraction of cell membrane*

Murine RAW264.7 cells were purchased from Shanghai Institute of Cell Biology, Chinese Academy of Sciences (Shanghai, China), and grown in a humidifying atmosphere with 5% $CO_2$ at 37 °C constant temperature. The medium was DMEM (Gibco, Grand Island, NY, USA) containing 10% fetal bovine serum and 1% penicillin–streptomycin (Gibco, Grand Island, NY, USA). The macrophages were exposed to hypotonic solution to burst the cell membrane and observed the morphological changes before and after breaking under bright field. Subsequently, Dounce homogenizer was used to disrupt completely the cell structure. The membranes were collected by density gradient centrifugation and stored at −80 °C for the next experiment.

### 2.5. *Preparation and characterization of NAL–SA-loaded macrophage-derived nanovesicles (NAL–SA–MVs)*

The above purified RAW264.7 cell membranes with 0.5% SA and 10 mg NAL were sequentially passed through 10 μm, 5 μm, 1 μm, 0.4 μm, and 0.2 μm of trail-etched polycarbonate film using an extruder. Subsequently, NAL–SA–MVs with uniform particle were formed and purified by glucan gelatin filtration chromatography (Sepharose CL-4B, Solarbio, Beijing, China).

The morphology of the NAL–SA–MVs was observed via transmission electron microscopy (TEM, JEM-1200EX; JEOL, Tokyo, Japan). The sizes, $\zeta$ potentials of MVs, SA–MVs and NAL–SA–MVs and stability study were monitored using a laser dispersion particle size analyzer (Nano-ZS90, Malvern, UK). Moreover, the drug content was recorded using an ultraviolet spectrophotometer (UV-2000, languages, Franksville, WI) at 230 nm. The following formula was used for calculating the encapsulation rate:

$$\textbf{Encapsulation rate}(\%) = (\textbf{encapsulated drugs}/\textbf{total amount of drugs}) \times 100\%$$

*In vitro* drug release studies were conducted using phosphate buffer solution (PBS, pH 6.8) as the release agent at 37 ± 0.5 °C. First, each sample (NAL–SA–MVs) was placed in a dialysis bag, and subsequently 4 ml of release medium was drawn at a predetermined time point, supplementing an equal volume of blank release the medium for keeping the volume constant in the meantime. The absorbance of NAL were measured using an ultraviolet spectrophotometer (UV-2000, LANGUAGES, FRANKVILI, WI) at 230 nm for calculating the cumulative release. The determination method of SA was as follows: 2 ml filtrate and 4 ml phloroglucinol (0.5%) were added to 5 ml concentrated hydrochloric acid under stirring, then the solution was placed in a boiling water bath for about 50 min. After color stabilization, a certain amount of water is added to bring the total volume to 25 ml. The SA content of sample solution were detected by ultraviolet spectrophotometer at 725 nm. All experiments were repeated thrice.

The pharmacokinetics of the NAL–SA–MVs and the free drug NAL were obtained by high-performance liquid chromatography (HPLC), and 6 SD rats (approximately 220 g) were randomly divided into two groups. These rats were fasted and allowed to drink freely for 12 h before the experiment. Respectively, the NAL–SA–MVs and the free NAL were injected into the rats through the tail vein. At 0.08 h, 0.25 h, 0.5 h, 12 h, 4 h, 6 h, 8 h, 10 h, 12 h and 24 h after the injection, the orbital venous blood was collected and placed in 1.5 ml eppendorf tubes containing heparin. All the above blood samples were centrifuged at 8000 r/min for 10 min, and each supernatant was stored at –20 °C in the refrigerator. 100 μl serum was added into 1 ml methanol solution containing the internal standard (5 μg/ml naltrexone solution). After 5 min of vortexing, the system was centrifuged at 10,000 r/min at room temperature for 10 min, and the supernatant was placed in sample bottles for HPLC analysis at 230 nm. 14% of methanol aqueous solution containing 86% of potassium dihydrogen phosphate was used as the mobile phases.

Toxicity assay of the MVs was performed at 5–25 μg/ml. $BV_2$ and VSC4.1 cells were inoculated on 96-well plates at 5000 cells/well. The MVs with different concentration were added, and then after 48 h, 20 μl of the MTT solution (5 mg/ml) and 150 μl DMSO was added orderly to each well. After 4 h the optical density (OD) value was measured at 490 nm using an microplate reader (DR−200B, Germany).

The marker proteins expression of RAW264.7 cell membranes was detected using western blot. Moreover, the following primary antibodies were used: F4/80 (1:1000, Abcam, Cambridge, UK) and CD11b (1:1000, Abcam, Cambridge, UK).

### 2.6. *The uptake and targeting evaluation of MVs*

NAL–SA–ReVs (erythrocyte–derived nanovesicles) was selected as the control. Erythrocyte of fresh blood was centrifuged at 3000 r/min for 10 min. Hypotonic solution was added and resuspend erythrocyte. The suspension system under ice bath rested for 30 min, and then the erythrocyte membrane was collected by centrifugation. Subsequently NAL–SA–ReVs were formed by successive extrusion. Fluorescein isothiocyanate (FITC) was used to label the NAL–SA–MVs and the NAL–SA–ReVs.

At the cell level, $BV_2$ and VSC4.1 cells were spread uniformly on a confocal dish, and the FITC labeled NAL–SA–MVs and the NAL–SA–ReVs were given to the cells and co-cultured. Subsequently, the excess material was washed with

PBS, then 4% paraformaldehyde (PFA) and 0.1% triton were added to fix and punch them. After washing, $\beta$-tubulin and DAPI was added for staining and kept moist in the confocal dish for uptake characterization by confocal fluorescence (Leica, Germany).

At the animal level, FITC-labeled NAL–SA–MVs and NAL–SA–ReVs were injected into C57 mice through the tail vein, and subsequently the spinal cord and major organs of different groups were dissected and removed at 3 h, 6 h, 9 h, 12 h, 24 h, 36 h and 48 h. Following this, the attached blood was washed with PBS, and the *in vivo* changes of the preparation were observed by an *in vivo* imaging system (IVIS Spectrum, PerkinElmer).

### 2.7. Analysis of free $Ca^{2+}$ content

BV2 cells were treated with lipopolysaccharide (LPS) (500 ng/ml) for 6 h and then administered different treatments. Diluted Fura-2AM was added separately to each group. After incubating for 1 h, its fluorescence intensity was observed by fluorescence microscope (Leica, Germany).

Transparent processing of spinal cord tissue: A transparent solution was composed of urea, 1-ethyl-3-(3-dimethylaminopropyl)carbodiimide, and triton. 0.5 cm of the spinal cord tissue near the site of injury was placed in the transparent solution and left overnight at 37 °C in a shaker.

Frozen spinal cord sections and transparent damaged spinal cord tissues were took and washed thrice with 0.9% saline for 5 min each time. The diluted Fura-2AM fluorescent probe was added and incubated for 50 min at room temperature, then washed again with 0.9% saline thrice for 5 min each time. The differences in the $Ca^{2+}$ content in the different groups of spinal cord tissues were observed under a fluorescent microscope (Leica, Germany).

### 2.8. Immunofluorescence analysis

In the cell experiment, the cells were treated to simulate the post-injury microenvironment. First, the cells were needed to be fixed with 4% PFA, and the spinal cord sections were needed to be circled by a PAP pen to prevent subsequent spiked samples from diffusing.

Subsequently, the samples were needed to be wash thrice with PBS, and dropped triton to disrupt the cell membrane for ensuring successful staining. The above samples was closed at room temperature by adding sheep serum for 2 h. A primary antibody was added, and the mixture was kept at 4 °C overnight. The next day, the cells were removed and washed thrice with PBS, following which a secondary antibody was added and incubated at room temperature for 2 h. The nuclei were stained with DAPI for 15 min. The cell fluorescence was observed under a fluorescence microscope (Leica, Germany), and the intensity was analyzed using ImageJ software.

### 2.9. Flow cytometry

VSC4.1 were spread uniformly in six-well plates and incubated in an incubator until 80% adhered to the wall. After different treatments, the supernatant was discarded, and 100 μl of the binding buffer was added to each group. Following this, the cells were stained with Annexin V-FITC/PI at room temperature for 10 min, and flow cytometry assessed the apoptosis of each group.

### 2.10. Western blotting

After anesthetizing, the spinal cord tissue of mice (approximately 1.5 cm) near the injury site were collected separately, and placed to RIPA lysate for protein extraction. In addition, the cells also were collected and subsequently used for protein extraction. BCA protein kit was used to quantify the protein concentration of the samples. The same protein amounts of different groups were added to the gels, and the protein were separated by electrophoresis using sodium dodecyl sulfate polyacrylamide gels. Subsequently, milk blocking solution (5%) was added and incubated for 2 h at room temperature, followed by the primary antibody was incubated overnight at 4 °C. The next day, the secondary antibody was added and incubated for 2 h at room temperature. It was observed by western blot imaging system and the images were analyzed using the Image J software. The western blot images should be convert the image to 8 bit type. Then the grayscale of the image background was homogenized to eliminate the effect of the image background. After inverting the black and white color of the image, measurement indicators area, mean gray value and integrated dendity should be selected and then set the measurement unit to a single pixel. Finally, the band was selected and measured the integrated optical density.

### 2.11. TUNEL assay

Frozen spinal cord sections were washed thrice with PBS, and 0.3% triton was added dropwise and incubated with the sections for 5 min at room temperature under dark conditions. And then a diluted TUNEL assay solution was added dropwise to the sections and incubated for 1 h at 37 °C under dark conditions. After washing with PBS, these sections were observed under a fluorescence microscope.

### 2.12. Behavior assessment

The basso mouse scale (BMS) [34,35] was used to evaluate the function recovery of SCI mice. The body stability standard is divided into 0–9 grade. Grade 0 represents the complete loss of hindlimb motor ability and grade 9 represents the complete recovery of hind limb motor function. One week before the experiment, the mice were placed on an open table and moved freely for 15 min. In the experiment, the BMS score every day were recorded and observe the change in the hind limbs functions of mice in a double blind situation. ($n = 5$).

### 2.13. Footprint experiment

Fourteen days after the successful modeling of the mice, the front and rear limbs were stained with two different colors, respectively, and subsequently the mice were placed on a paper to walk for recording the footprint. The recovery of the mice hind limbs was evaluated according to the degree of coordination and continuity of the hind foot footprints ($n = 5$).

### 2.14. Nissl staining

The mice were intraperitoneally injected with 1% pentobarbital sodium for depth anesthesia. Subsequently 0.9% normal saline and 4% PFA were used, respectively, to flush the blood and fixed tissues by intracardiac injection. The mice spinal cord in each group were collected, washed with PBS, soaked in 4% PFA, and subsequently dehydrated with ethyl alcohol. The spinal cord tissues were then embedded with paraffin and sectioned. A spinal cord slice was dried, and subsequently it was soaked in a solution containing chloroform and ethanol in a ratio of 1:1 for 24 h. Then it was placed and soaked in turn with different concentrations of ethanol for dewaxing. The cresyl violet solution and nissl differentiation solution was used, respectively, for staining of the slice. After dehydration and transparency with anhydrous ethanol and xylene, these slices were sealed with a neutral gum and observed the number of neurons and nissl body by microscope (DMI4000B, Leica, Wetzlar, Germany).

### 2.15. Hematoxylin–eosin staining

After perfusion, the main organs of the mice were taken out, paraffin embedded and sectioned in accordance with the above methods. Then it was dewaxed, and hematoxylin dyeing liquid was added and co-incubated with the organs for 5–20 min, following the eosin dye solution was added and continued for staining. And then the sections were dehydrated in the different concentrations of alcohol and xylene. Finally, these sections were sealed with a neutral gum, and the changes in the organ sections in each group were observed to estimate the safety of the preparations.

### 2.16. Data analysis

SPSS 21.0 was used for data analysis. All experimental results were expressed as mean standard deviations by the Shapiro-Wilk test, and the difference between the two groups was statistically significant ($P < 0.05$). The Mann-Whitney U test was used for two-group comparisons. One-way ANOVA and Bonferroni post hoc tests were used to compare more than two groups.

## 3. Results and discussion

### 3.1. Characterization of NAL–SA–MVs

The preparation process of the NAL–SA–MVs is mainly presented in Scheme 1. First, isolated RAW264.7 cell membranes are mixed with the NAL and SA solution. Subsequently, the NAL–SA–MVs are obtained after continuous extrusion through polycarbonate membranes. A glucan gel column is used for purification, and tail intravenous injection is selected as the administration way of the SCI mice. The NAL–SA–MVs can target injured sites and play the role of reducing the free $Ca^{2+}$ concentration, inhibiting inflammation and anti-apoptosis. The TEM images of MVs was shown in Fig. S2, which exhibited the spherical structure. A TEM image (Fig. 1A) showed that the NAL–SA–MVs possessed a spherical structure of size of approximately 134 ± 11 nm. The particle size analysis results were consistent with the TEM images. The results (Fig. 1B) exhibited that size of MVs was about 80 ± 12 nm. By comparison, the particle size of the SA–MVs reached 112 ± 8 nm. After loading the NAL, the diameter increased to 143 nm in comparison to that of MVs. The slight increase in the particle size was caused by the encapsulation of the SA and the NAL. The $\zeta$ potential results (Fig. 1C) revealed that the SA–MVs (−57.9 ± 3.7 mV) decreased approximately 23.9 mV in contrast to the MVs (−34.0 ± 6.3 mV). The decrease in the potential was due to the negative charge on the SA surface. After loading the NAL, the NAL–SA–MVs (−55.3 ± 5.1 mV) were almost not changed compared to the SA−MVs because NAL had no charge. The 7 d stability test (Fig. 1D) showed that the particle size and $\zeta$ potential of the NAL–SA–MVs did not change significantly, indicating that the drug delivery system was stable. In the drug delivery system, NAL played a significant role in inflammation and apoptosis as a drug. However, the short half-life of NAL influenced the therapeutic effect severely [36]. As endogenous drug carrier materials, MVs can prolong the circulatory time of NAL *in vivo* and improve drug bioavailability. The encapsulation rate of NAL and SA was 82.07% ± 3.27% and 72.13% ± 2.61% in the sample, respectively. The *vitro* drug release test (Fig. 1E) showed the cumulative release amount of NAL and SA at 12 h was 40.5% ± 3.64% and 21.31% ± 1.05%. As a natural biomacromolecule, SA is not easily released in the cell membrane vesicles. The release results revealed release behavior of SA and NAL presented sustained release effect, which was beneficial to reduce drug loss during systemic circulation and made more NAL and SA reach to the site of injury. Under the action of lysosome, the membrane structure of NAL-SA-MVs was destroyed, which caused a large amount of NAL and SA release in the lesion site. This will maximize the therapy efficacy of SA and NAL. The plasma concentration curve and the pharmacokinetic parameters (Fig. 1F) exhibited that $MRT_{0\text{-}t}$ of the free NAL was 1.694 ± 0.11 h, and that of the NAL–SA–MVs was 10.106 ± 0.07 h. Moreover, the $AUC_{0\text{-}t}$ (1740.897 ± 30.972 ng/ml•h) of the NAL–SA–MVs was approximately 2 times as big as the free NAL (886.397 ± 38.353 ng/ml•h). The pharmacokinetic test results demonstrated that NAL in the NAL–SA–MVs displayed

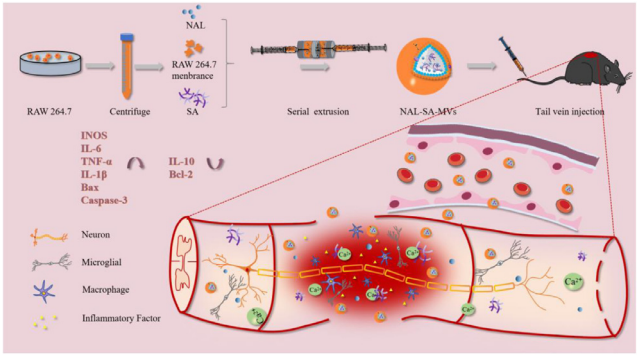


**Scheme 1 – Sodium alginate and naloxone loaded macrophage-derived nanovesicles preparation and spinal cord injury therapy.**

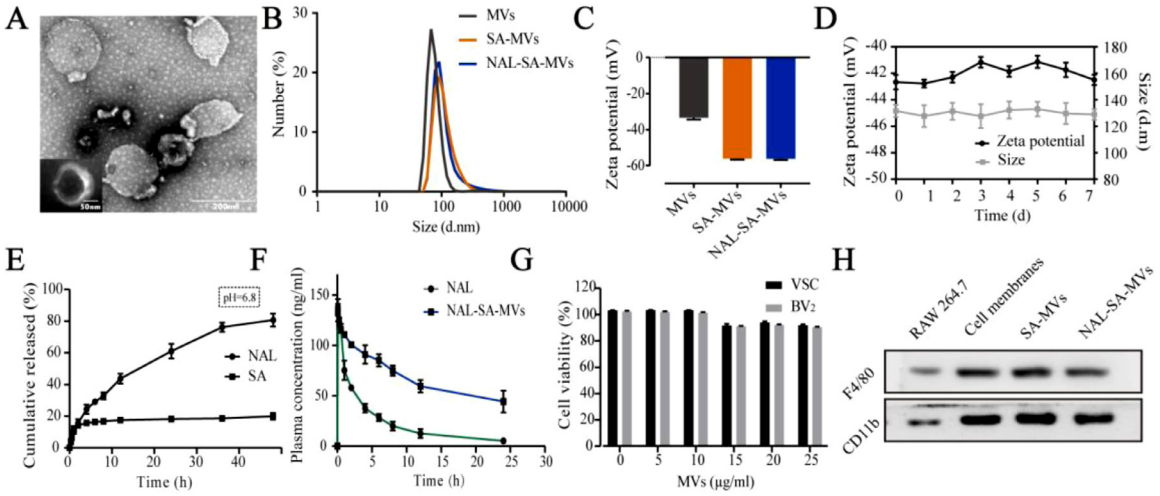


**Fig. 1 – The characterization of NAL-SA-MVs. (A) TEM imaging of NAL-SA-MVs. (B) The DLS size distribution diagrams of MVs, SA-MVs, NAL-SA-MVs. (C) The ζ potential distribution of MVs, SA-MVs, NAL-SA-MVs. (D) 7 d stability test of NAL-SA-MVs. (E) The *vitro* release assay of NAL and SA. (F) The pharmacokinetics of free NAL and NAL-SA-MVs *in vivo*. (G) The cytotoxicity of blank MVs in VSC4.1 and $BV_2$. (H) Western blotting analysis of protein markers of RAW264.7, RAW264.7 cell membranes, SA-MVs and NAL-SA-MVs. All data represented the mean ± SD ($n = 3$).**

sustained release and long-lasting effects. The toxicity of the MVs and NAL-SA-MVs was evaluated by the MTT analysis (Figs. 1G and S3). The survival rates of the $BV_2$ and VSC4.1 cells were more than 85% after treated with different concentrations of MVs and NAL-SA-MVs about 24 h, respectively. It demonstrated the MVs and NAL-SA-MVs have good biosafety. The western blotting results (Fig. 1H) exhibited that the characteristic macrophage marker proteins, F4/80 and CD11b, were less expressed in RAW264.7 cell group, but more expressed in RAW264.7 cell membranes, SA–MVs and NAL–SA–MVs groups. It indicated that the RAW264.7 cell membranes had been successfully extracted and the surface protein properties of the macrophage did not change during preparation. The images of RAW264.7 cells before and after bursting in hypotonic solution also indirectly proved the feasibility of membrane extraction process in Fig. S1. The morphology changes of cells before and after the rupture could be clearly seen in the open field of the microscope. Compared with normal cells, cells in the hypotonic solution became significantly larger and burst. MVs can play an important part in inflammation targeted therapy owing to the protein and ribonucleic abundance on the macrophage membrane surface. Therefore, it has a homologous tendency to the macrophages of the inflammation site, which indicates its suitability as a drug carrier to target inflammation.

### 3.2. *The uptake and targeting evaluation of MVs*

In this experiment, we chose the representative cells of inflammation ($BV_2$) and apoptosis (VSC4.1) as the research objects to study the therapeutic action of the NAL–SA–MVs. ReVs were selected as control group in cellular uptake and targeting evaluation studies. Based on the *in vitro* cell uptake experiments (Fig. 2), the difference between the MVs and ReVs uptake by $BV_2$ and VSC4.1 was clearly observed. The uptake of the ReVs by the $BV_2$ cells was 31.07% ± 2.75%, whereas that of the MVs reached 75.32% ± 1.97%. Similarly, the uptake of the ReVs by the VSC4.1 was 27.19% ± 3.05%, whereas that of the MVs by the VSC4.1 reached 83.37% ± 2.46%. Similar trends indicated that the MVs could be uptake and function well in the $BV_2$ and VSC4.1 cells. The results showed that MVs could be taken up by the VSC4.1 and $BV_2$ at the cellular level. To confirm the targeting ability of the MVs, the mice were injected with FITC-labeled MVs and ReVs, respectively. Subsequently, we used small animal live imaging (Fig. 2) to observe the fluorescence intensity of the mice spinal cord at 3 h, 6 h, 9 h, 12 h, 24 h, 36 h and 48 h. The ReVs group showed almost no fluorescence at 3 h, and presented a gradual increase of intensity with time. The fluorescence intensity reached the peak at 12 h. However, the duration was short. It founded that ReVs had very little aggregation although the BBB/BSCB was destroyed for the SCI mice. In contrast, the fluorescence intensity at the injured site in the MVs group presented faint fluorescence at 3 h and gradually increased with time. At 12 h, the intensity reached maximum and lasted for more than 48 h. And the ratio of fluorescence intensity between spinal cord and liver in MVs group was about 2.5 times that in ReVs group (Fig. S4). Macrophages were recruited from the entire body to the site of injury because of the chemokines produced by the inflammation after SCI, and strongly accumulated at the injury lesions. Therefore, the results suggested that MVs could target to the inflammatory site and cause a long-acting therapeutic effect. The major organs of the two groups were collected and subjected to fluorescence imaging (Fig. 2). It showed the metabolism was mainly through the liver.

### 3.3. *Effect of NAL–SA–MVs on reducing free $Ca^{2+}$*

When the spinal cord is subjected to a mechanical collision or compression, it can lead to BBB/BSCB destruction, bleeding and microvascular thrombosis at the site of lesion. Subsequently, it can result in further ischemic and hypoxic

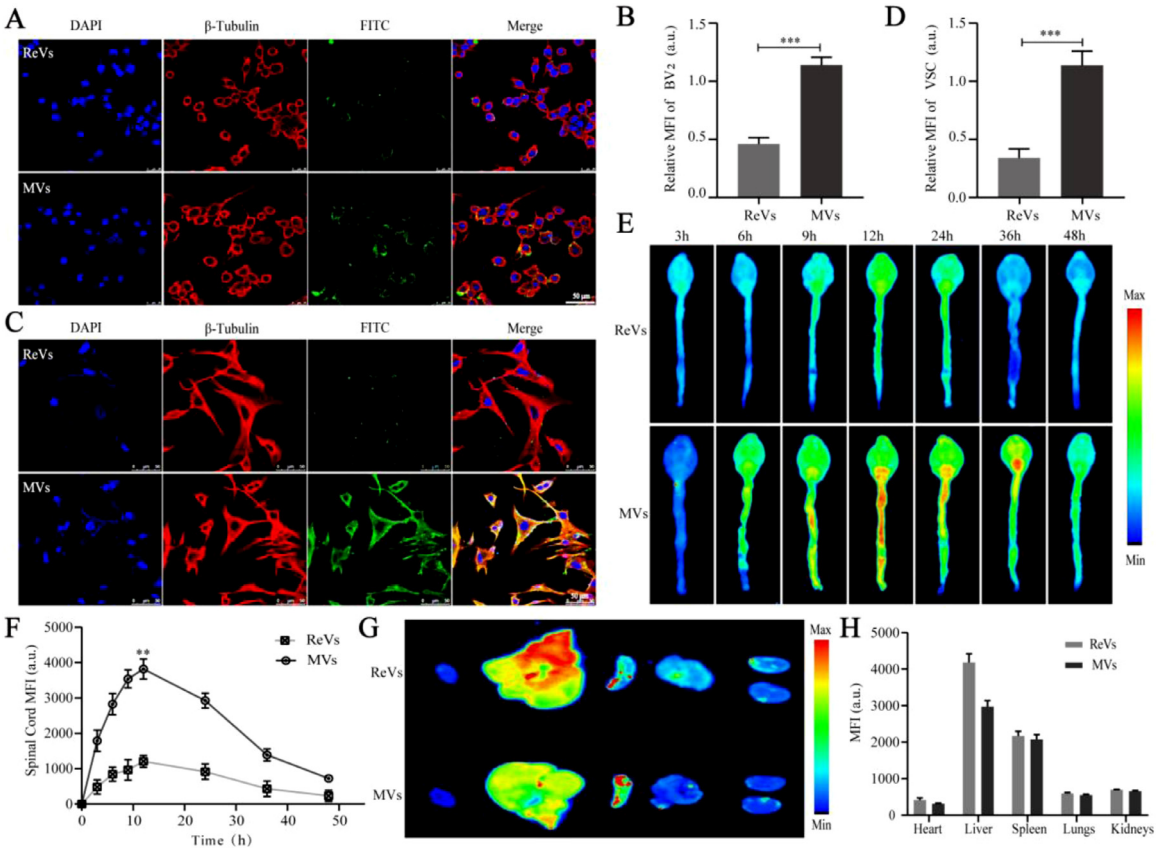


**Fig. 2 – The uptake of NAL-SA-MVs *in vitro* and the targeting of NAL-SA-MVs *in vivo*. (A, B) Confocal fluorescence imaging of $BV_2$ cells treated with FITC-ReVs and FITC-MVs. FITC-ReVs/FITC-MVs (green), nucleus (blue) and cell membrane (red). (C, D) Confocal fluorescence imaging of VSC4.1 cells treated with FITC-ReVs and FITC-MVs. FITC-ReVs/FITC-MVs (green), nucleus (blue) and cell membrane (red). (E) The spinal cord fluorescence imaging of SCI mice after FITC-ReVs and FITC-MVs injected by tail vein, respectively, at different time points. (F) Fluorescence quantitative analysis of spinal cord in different groups over time. (G) The fluorescence imaging of the major organs (heart, liver, spleen, lung and kidney) from different groups mice at 12 h after tail vein injection. (H) Fluorescence quantitative analysis of organs in different groups. All data represented the mean ± SD ($n = 3$). *$P < 0.05$, **$P < 0.01$, ***$P < 0.001$.**

damage to the spinal cord. The above caused biofilm depolarization, opening of the calcium channels, and inward $Ca^{2+}$ flow. Concurrently, the concentration of $Ca^{2+}$ increase in the release pool of the intracellular $Ca^{2+}$ (chonmitodrial and endoplasmic reticulum), *i.e.*, there is an increase in the intracellular release of $Ca^{2+}$. Moreover, large amounts of $Ca^{2+}$ in the cell cannot be pumped out of the body normally because of lack of ATP. Finally, the cell $Ca^{2+}$ regulation mechanism under the physiological state loses its function. $Ca^{2+}$ overload caused the release of inflammatory factors, cell aging, and even cell death [37–39]. Studies showed that SA can chelate with free $Ca^{2+}$ to reduce the concentration of free $Ca^{2+}$, which can alleviate the secondary damage after SCI. Naloxone can competitively block endogenous opioids, reverse ATPase activity, increased cAMP content and $NA^{+}$–$K^{+}$–ATPase activity. These processes were beneficial to inhibit $Ca^{2+}$ influx, increase cell membrane stability, and improve $Ca^{2+}$ plasma disorder in neuron cells. Therefore, the combination of SA and NAL can play a better synergistic effect.

$BV_2$ was treated with LPS to simulate the $Ca^{2+}$ overload phenomenon in an injury microenvironment (Fig. 3). The results showed that the PBS group expressed strong green fluorescence, indicating a high level of free $Ca^{2+}$. In contrast, the SA–MVs group presented a relatively weak fluorescence intensity, showed that SA could bind with free $Ca^{2+}$ and significantly reduce its concentration. The NAL–SA–MVs group had the strongest ability to reduce the green fluorescence intensity, which demonstrated that it had the best decrease effect of free $Ca^{2+}$. Fluorescence of the tissue further confirmed the above conclusion. At the animal level, it also used the Fura-2AM fluorescent probe to detect the levels of free $Ca^{2+}$ (Fig. 3). The collected corresponding spinal cord tissue after administering different treatments to the SCI mice was transparented and sectioned, respectively. The sham group almost had no green fluorescence, whereas the SCI group fluorescence intensity was the highest. Concurrently, the NAL and SA–MVs groups had a slight reduction in the green fluorescence. The NAL–SA–MVs group had the strongest ability to reduce the fluorescence intensity. Reducing the

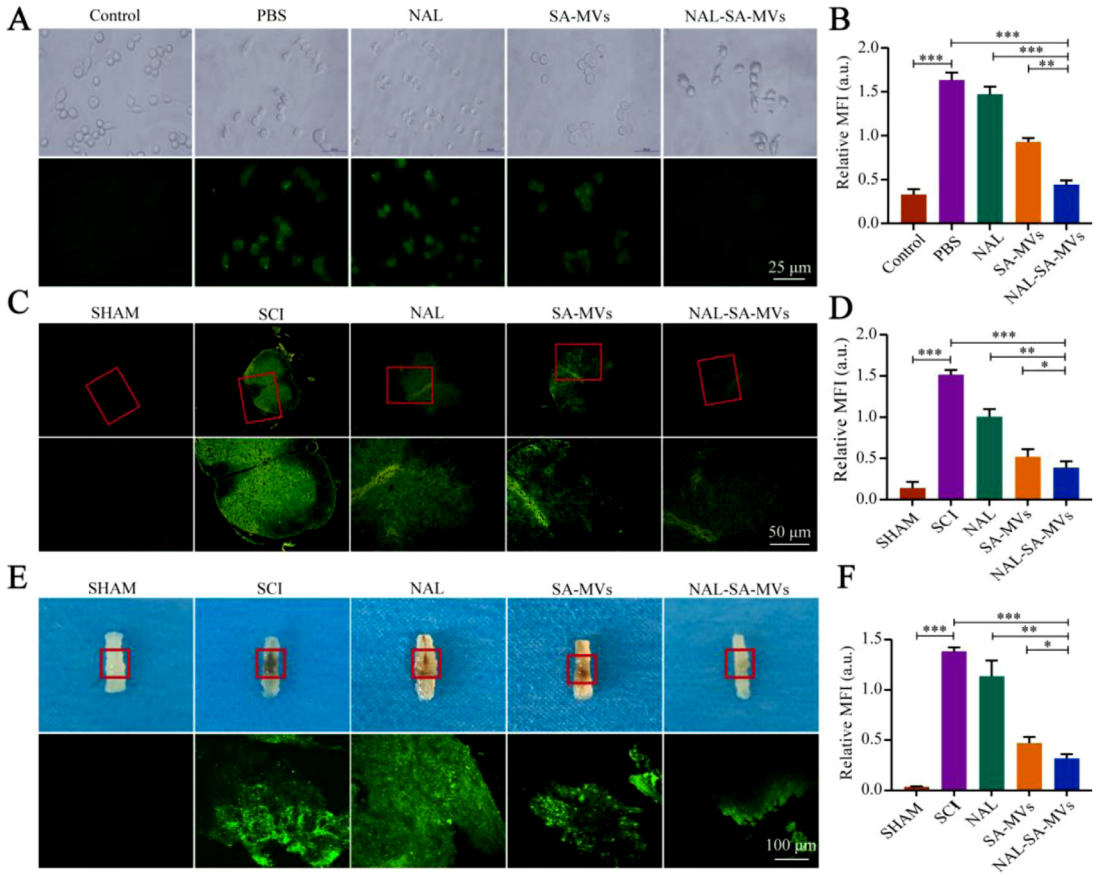


**Fig. 3 – SA binds to $Ca^{2+}$ and reduces the concentration of free $Ca^{2+}$ in the damaged microenvironment. (A, B) Intracellular free $Ca^{2+}$ was determined by Fura-2AM fluorescent probe and its statistical analysis. (C, D) Determination and statistical analysis of free calcium ion concentration in injured spinal cord tissue sections by Fura-2AM fluorescent probe. (E, F) Two-photon detection of free calcium ion concentration in hyaline spinal cord and its statistical analysis. All data represented the mean ± SD ($n = 3$ per group). *$P < 0.05$, **$P < 0.01$, ***$P < 0.001$.**

$Ca^{2+}$ concentration at the site of injury is important for to alleviating inflammatory and neuron damage.

### 3.4. *Anti-inflammatory effect in vitro and vivo*

Many inflammatory factors were released into the damaged microenvironment after SCI, resulting in an uncontrollable inflammatory response [40–42]. The factors included pro-inflammatory factors iNOS, TNF-$\alpha$, IL-1$\beta$, and IL-6 as well as anti-inflammatory factor IL-10 [43–45]. When the expression of the pro-inflammatory factors elevated, the level of inflammation in the injured spinal cord also increased. Concurrently, the increase of anti-inflammatory factors indicated inflammation decrease. However, pro-inflammatory and anti-inflammatory factors were significantly imbalanced in the microenvironment of the SCI. Therefore, controlling the expression of pro-inflammatory factors and promoting the secretion of anti-inflammatory factors will effectively decrease the inflammatory levels in a damaged microenvironment. To test the anti-inflammatory capabilities of the NAL–SA–MVs at the cell level, we conducted immunofluorescence and western blot assays. INOS was mainly derived from microglia cells after SCI. Studies showed that iNOS could promote early SCI by increasing the inflammatory response. $BV_2$ cells were first treated with LPS for 6 h to simulate the inflammation environment, and then with the corresponding therapy, the immunofluorescence of iNOS (Fig. 4) showed that the control group had no fluorescence, whereas a strong green fluorescence was expressed in the PBS group. This suggested that the $BV_2$ cells were in the strongest inflammatory state after LPS treatment. The NAL and SA–MVs groups could reduce the expression of the iNOS. However, the effect was limited. The fluorescence intensity of the NAL–SA–MVs group was approximately 1/4 of the SCI group. Immunofluorescence results showed that the NAL–SA–MVs could significantly reduce the fluorescence intensity compared with the NAL and SA–MVs groups, indicated that the NAL–SA–MVs had a great anti-inflammatory effect. Western blot characterization (Fig. 4) determined the expression levels of iNOS, IL-6, and IL-10, which further verified the above results. The expressions of pro-inflammatory factors iNOS and IL-6 were very low in the control group, whereas in the PBS group, they had the highest expression. In comparison, the NAL and SA–

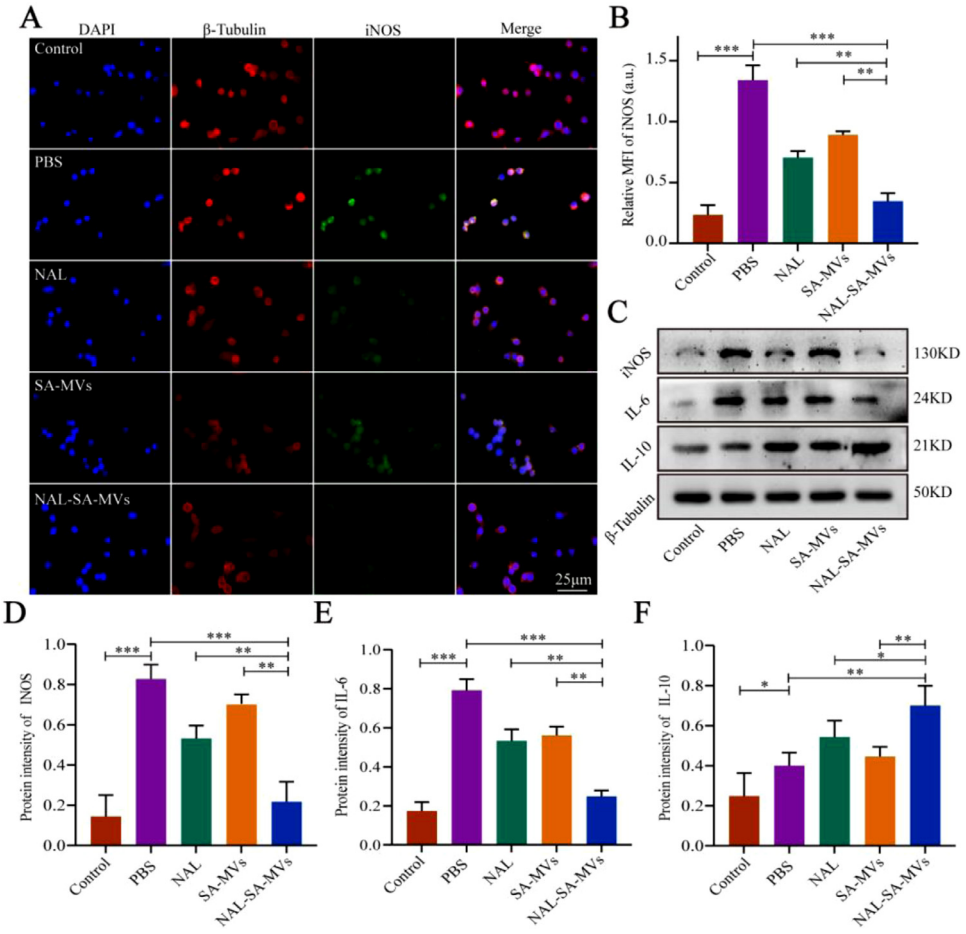


**Fig. 4 – NAL-SA-MVs inhibited the secretion of inflammatory mediators and achieved anti-inflammatory effect *in vitro*. (A) Fluorescence microscopy images for immunofluorescence staining of $BV_2$ cells were untreated, treated with PBS, NAL, SA-MVs and NAL-SA-MVs. Cell nuclei were stained with DAPI (blue), cell cytoskeleton was stained with $\beta$- tubulin (red), pro-inflammatory protein were stained with iNOS (green). (B) Fluorescence quantitative analysis in different groups. (C) Western blot detection of the inflammatory factors (iNOS, IL-6, IL-10) released by $BV_2$ cells in different groups. (D–F) Quantitative protein expression statistical analysis of (iNOS, IL-6 and IL-10 in figure C. All data represented the mean ± SD ($n = 3$ per group). *P < 0.05, **P < 0.01, ***P < 0.001.**

MVs groups showed a reduction in the expression level, indicated that both had anti-inflammatory effects to some extent. The NAL–SA–MVs group had the highest reduction expressions of the inflammatory factors and the strongest anti-inflammatory effect. IL-10 can suppress TNF-$\alpha$ and IL-6 through activated macrophages and played a very important balancing role in the regulation of pro-inflammatory cytokine overexpression after SCI. The results of the anti-inflammatory factor (IL-10) was inversely validated the anti-inflammatory effect of the NAL–SA–MVs group, and the expression of IL-10 was the strongest among all other groups.

To further investigate the inhibitory effect of inflammation of the NAL–SA–MVs after SCI, we used western blot and immunofluorescence to verify the expression level of inflammatory cytokines in animal level. Among them, western blot was used to measure the expression levels of iNOS, IL-6, TNF-$\alpha$, IL-1$\beta$ and IL-10 in the spinal cord tissue and evaluate the inflammation level in the injury site (Fig. 5). The content of pro-inflammatory factors (iNOS, IL-6, TNF-$\alpha$, and IL-1$\beta$) was extremely low in the sham group and highest in the SCI group. It was slightly reduced in both NAL and SA–MVs groups, and had the most decrease in the NAL–SA–MVs group. The sham and SCI groups showed weak IL-10 expression. The NAL and SA–MVs groups had relatively higher expressions. Moreover, the NAL–SA–MVs group showed the highest increase, indicated that it had the best anti-inflammatory effect. It validated that the NAL–SA–MVs could notably reduce the expression of pro-inflammatory factors (iNOS, IL-6, IL-1$\beta$, TNF-$\alpha$) in the post-injury microenvironment and also promote anti-inflammatory factors (IL-10) expression compared with the NAL and SA–MVs groups. Immunofluorescence intensity and statistical analysis of IL-1$\beta$ in the spinal cords of the different treatment groups after SCI were consistent with the western blot results. The value (Fig. 5) level of IL-1$\beta$ in the sham group had a very low expression, whereas in the SCI group, it was approximately five times as strong as in the sham group, showing a high level of inflammation at the injured site. The fluorescence intensity of the NAL and

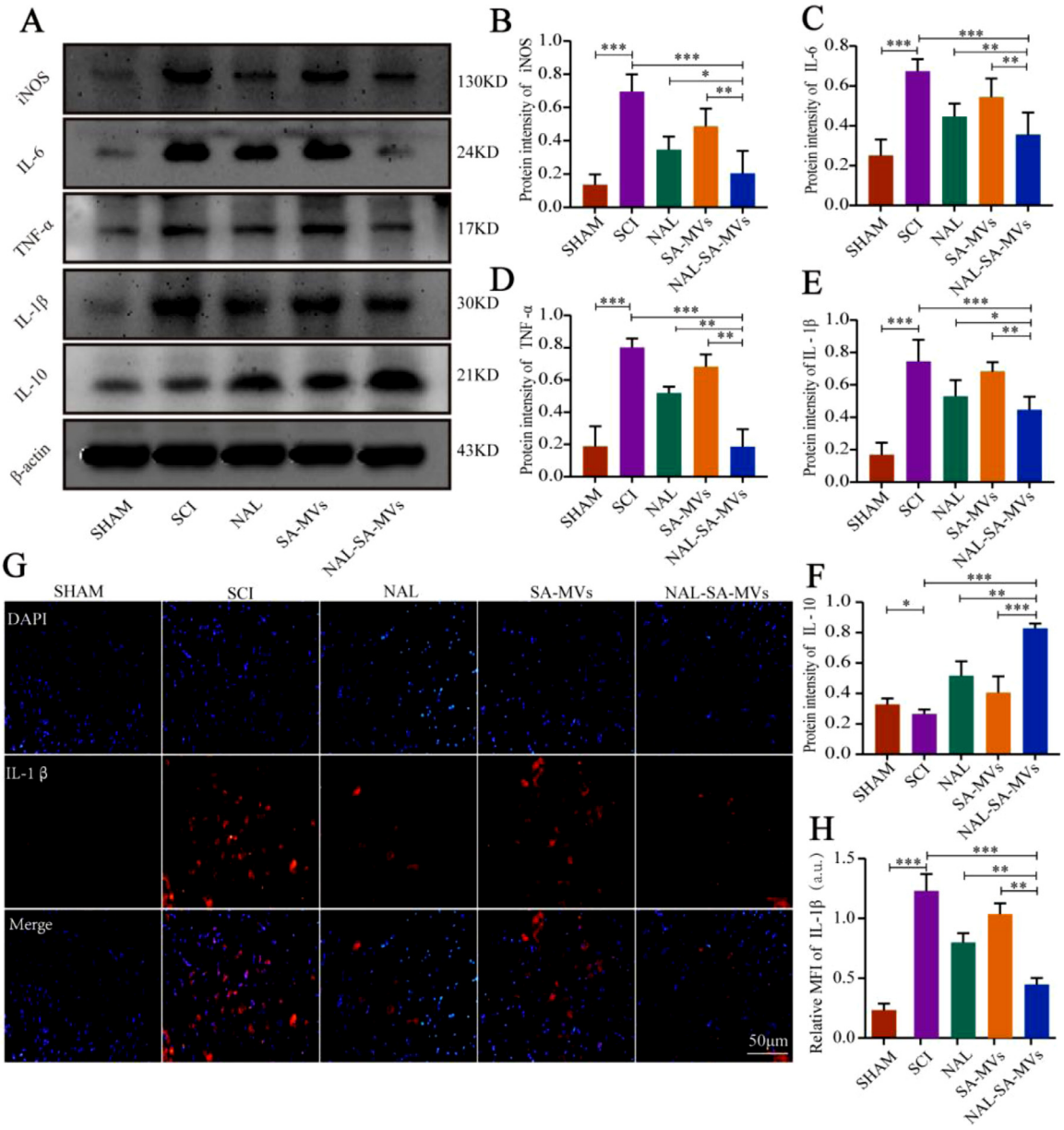


**Fig. 5 – NAL-SA-MVs inhibited the inflammatory response at the site of injuried spinal cord. (A) Western blot detection of the inflammatory factors (iNOS, IL-6, TNF-α, IL-1β, IL-10) from spinal cord tissue of different groups. (B-F) Quantitative protein expression statistical analysis of iNOS, IL-6, TNF-α, IL-1β, IL-10 in Fig. 5A. (G, H) Fluorescence microscopy images for immunofluorescence staining of spinal cord tissue sections. Cell nuclei were stained with DAPI (blue), pro-inflammatory protein were stained with IL - 1β (green). All data represented the mean ± SD ($n = 3$ per group). *P < 0.05, **P < 0.01, ***P < 0.001.**

SA-MVs groups decreased to some extent. Moreover, the IL-1β value decreased most significantly in the NAL–SA–MVs group.

### 3.5. *Anti-neuronal cell apoptosis effect in vitro and vivo*

SCI can also lead to massive apoptosis of neurons [46,47]. Apoptosis is an active process of cell death occurring under certain physiological or pathological conditions [48]. Among the apoptosis regulating factors, the Caspase and Bcl-2 family generated the most interest. Decreasing the Caspase-3 expression level is one of the important pathways to slow down the secondary SCI. Moreover, Bax and Bcl-2 are a pair of key regulatory factors with opposite functions in apoptosis [49,50]. The increase in Bax, Caspase-3, and Bax/Bcl-2 indicated an increased proportion of neuronal apoptosis after SCI [51]. The increase in the anti-apoptotic factor (Bcl-2) could alleviate the level of neuron apoptosis. To investigate the anti-apoptotic effect of the NAL–SA–MVs, we performed flow cytometry, immunofluorescence, and western blot tests *in vitro*. Flow cytometry detected the percentage

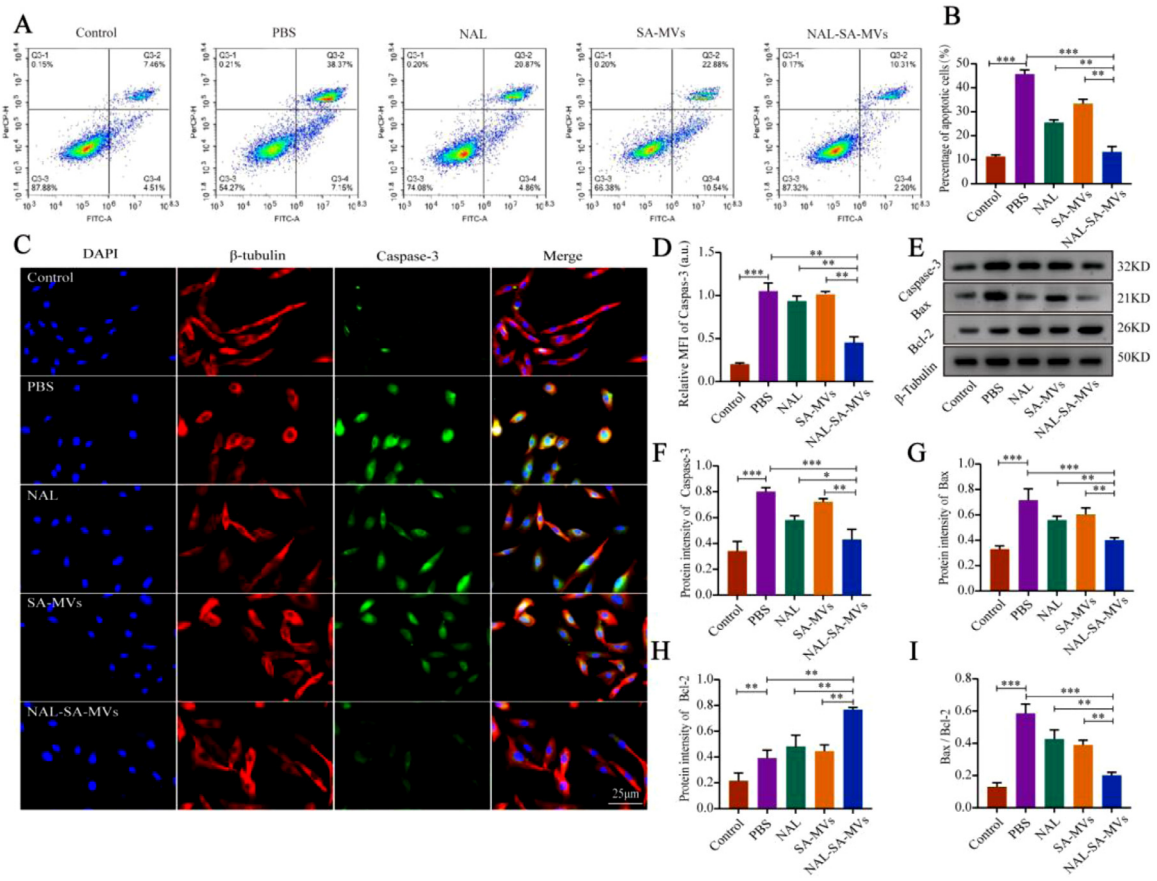


**Fig. 6 – NAL-SA-MVs can inhibit the expression of apoptotic factors and has anti-apoptotic effect *in vitro*. (A, B) Representative flow cytometry analysis of the proportion of apoptotic cells in each treatment group and the corresponding quantitative analysis. (C, D) Fluorescence microscopy images of VSC4.1 cells were untreated and treated with PBS, NAL, SA-MVs, NAL-SA-MVs. Cell nuclei were stained with DAPI (blue), cell cytoskeleton was stained with $\beta$ - tubulin (red), pro-apoptotic protein were stained with Caspase-3 (green). (E) Western blot detection of the apoptotic factors (Caspase-3, Bax, Bcl-2) released by VSC4.1 cells in different groups. (F–I) Quantitative protein expression statistical analysis of Caspase-3, Bax, Bcl-2 and Bax/Bcl-2 in figure E. All data represented the mean ± SD ($n = 3$ per group). *P < 0.05, **P < 0.01, ***P < 0.001.**

of the apoptotic cells (Fig. 6). The control group was only 11.93% ± 1.2%, and the PBS group was 45.34% ± 2.1%. Under the action of NAL, the apoptosis rate was reduced to 25.48% ± 1.7%, indicated that NAL had a neuroprotective effect. In contrast, the apoptosis rate was reduced to 33.58% ± 1.5% in the SA–MVs group. Although both the NAL and SA–MVs groups showed the effect of anti-apoptotic effect, it was not enough to achieve satisfactory effect. The NAL-SA-MVs group significantly decreased the proportion of apoptotic cells compared with the previous two groups. It were approximately 12.51% ± 0.8%, which was approximately 33% lower than that of the PBS group. This demonstrated that the NAL–SA–MVs group had the strongest neuroprotective and anti-apoptotic effects. The results of the immunofluorescence experiment were consistent with the above trends (Fig. 6). The sham group had a very low expression of Caspase-3. The high expression of green fluorescence in the PBS group indicated that the VSC4.1 entered the apoptotic state. The NAL and SA–MVs groups had relatively weak green fluorescence, and moreover interestingly, the NAL–SA–MVs group had the strongest reduction expression intensity. The above conclusions were further confirmed by western blot of the expression levels (Fig. 6). The expressions of Bax, Caspase-3 and Bax /Bcl-2 were extremely low in the control group, and highest in the PBS group. The NAL and SA–MVs groups showed relatively weak expressions, and the NAL–SA–MVs had the strongest therapeutic effect. The results of Bcl-2 were very low in the control group and slightly increased in the PBS group. In comparison, the NAL and SA–MVs groups showed an increase in the protein expression to some extent. Based on the above results, the NAL–SA–MVs group had the highest expression, indicating it had the best anti-apoptotic effect.

Western blotting analysis, TUNEL and immunofluorescence were conducted to study the anti-apoptotic effect of the NAL–SA–MVs in animal level. The expression levels of pro-apoptosis proteins Bcl-2, Bax, Bax/Bcl-2 and Caspase-3 were shown in Fig. 7. Compared with the PBS group, the NAL, SA–MVs and NAL–SA–MVs had significantly lowed expression levels of the pro-apoptosis factors, indicated that they had anti-apoptotic effects, and the NAL–SA–MVs had the optimum effect. The results were further verified by immunofluorescent

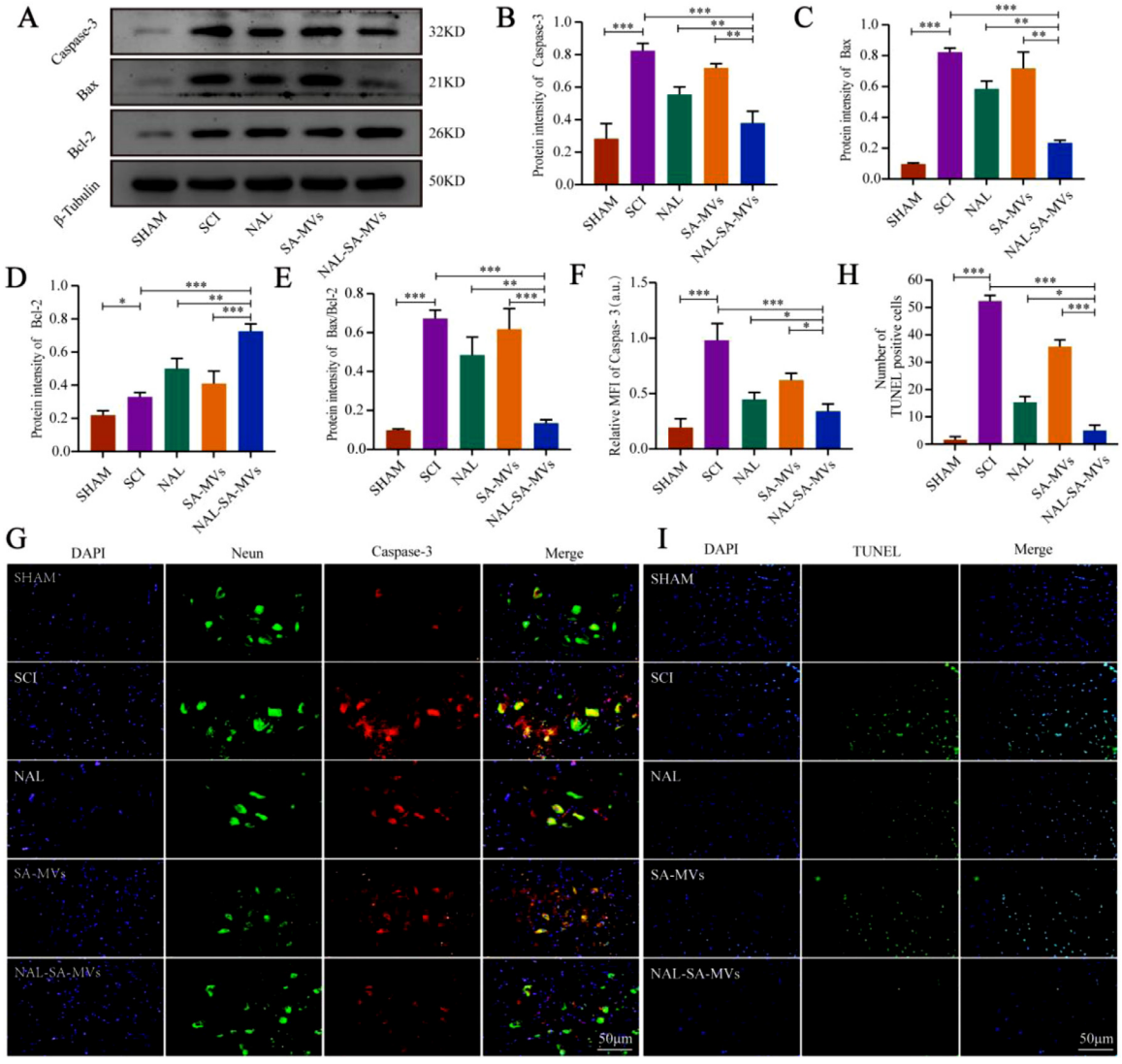


**Fig. 7 – NAL-SA-MVs inhibited apoptosis after spinal cord injury in mice. (A) Western blotting detection of the cytokines (Caspase-3, Bcl-2, Bax) from spinal cord tissue of different groups. (B–E) Quantitative protein expression statistical analysis of Caspase-3, Bax, Bcl-2 and Bax/Bcl-2 in Fig. 7A. (F, G) Fluorescence microscopy images of spinal cord tissue sections of sham, SCI, NAL, SA-MVs and NAL-SA-MVs. Cell nuclei were stained with DAPI (blue), neurons were stained with neun (green), and apoptin were stained with Caspase-3 (red). (H, I) Fluorescence microscopy images and statistical analysis of TUNEL-DAPI assay. All data represented the mean ± SD ($n = 3$ per group). *$P < 0.05$, **$P < 0.01$, ***$P < 0.001$.**

double staining of Caspase-3/neuron (Fig. 7). The fluorescence expression was lowest in the sham group and highest in the SCI group. Compared to the PBS group, the apoptotic protein expressions of the NAL, SA–MVs and NAL–SA–MVs were lower, indicated that they had anti-apoptotic effects. Among them, the NAL–SA–MVs had the most decrease in the fluorescence intensity. TUNEL fluorescence of the spinal cord tissue (Fig. 7) showed that NAL and SA–MVs also led to improvements to some extent compared to the SCI group. The NAL–SA–MVs group had the best anti-apoptotic effect and that its fluorescence intensity was approximately 1/5 of the SCI group, which further confirmed the above conclusion. The above results demonstrated that the NAL–SA–MVs had the effects of reducing the free $Ca^{2+}$ concentration, inflammation inhibition and neuroprotection.

### 3.6. *NAL–SA–MVs protect neurons and promote motor function recovery after SCI*

Fig. 8A showed the wound surface in the SCI model process. The BMS score was used to evaluate the motor recovery of the SCI mice (Fig. 8B). The scores of the NAL, SA-MVs and NAL–SA–MVs groups were significantly higher than those of the SCI group at 14, 21 and 28 d. After SCI, the weights (Fig. 8C) of the mice in the NAL and SA–MVs groups decreased slightly and gradually regained after treatment. The therapeutic effect of the NAL–SA–MVs group was the most obvious. However, it did not return to the weight level before injury. It demonstrated that the curative effect of the NAL–SA–MVs was definite. The 28 d footprint test of SCI mice (Fig. 8)

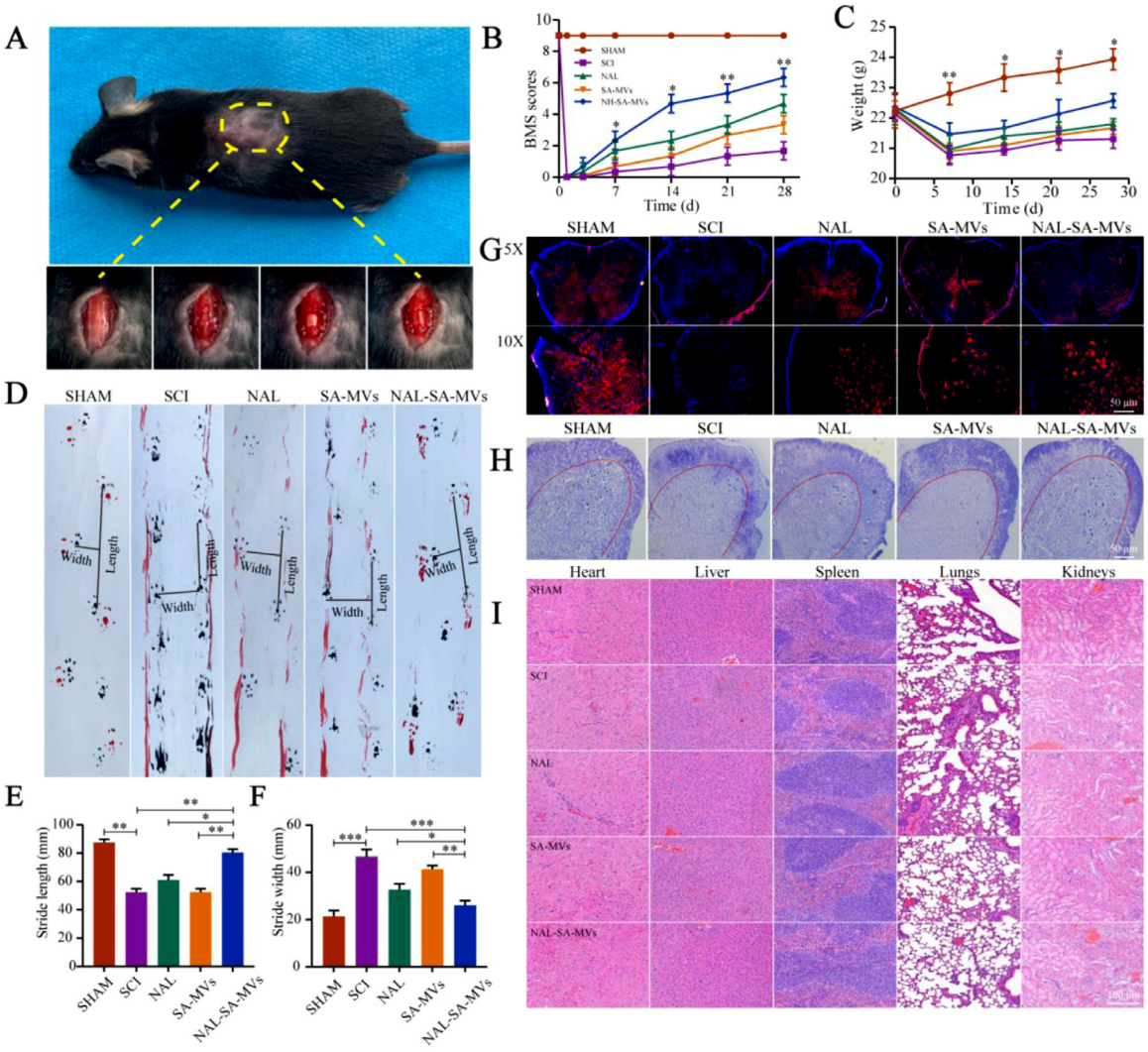


**Fig. 8 – NAL-SA-MVs could promote the survival of neurons and the recovery of motor function in mice after spinal cord injury, and the evaluation of the preparation safety. (A) The wound surface of a mouse in the process of SCI model. (B) Statistical analysis of BMS scores in different groups before and after spinal cord injury in mice. (C) Statistical analysis of body weight of mice before and after spinal cord injury. (D) Footprints of SHAM, SCI, NAL, SA-MVs and NAL-SA-MVs group. The forepaws and hindpaws of each group were stained, respectively, with black and red dye. (E, F) The statistical analysis of step length (SL) and stride width (SW). (G) Neun-labeled neurons at 5 x and 10 x of the different groups. (H) Number of surviving neurons at 7d after spinal cord injury in each group by Nissl staining. (I) HE staining of heart, liver, spleen, lung and kidney tissue sections of each group for safety evaluation. All data represented the mean ± SD ($n = 5$). *$P < 0.05$, **$P < 0.01$, ***$P < 0.001$.**

exhibited severe incoordination and dragging. These mice had shorter and wider strides. In the NAL and SA–MVs groups, the coordination and hindlimb strength problem was relieved to some extent. The step length increased, and the step width of the mice became narrow. However, it still did not reach the normal level before modeling. Moreover, the NAL–SA–MVs group displayed the best recovery effect. The Nissl staining and neuron fluorescence results was used to observe the effect of the NAL–SA–MVs on the survival of the motor neurons cells after SCI (Figs. 8, and S5 & S6). The number of neurons in the SCI group sharply decreased and even disappeared, and the number of neurons in the NAL, SA–MVs and NAL–SA–MVs groups increased. Among them, the NAL–SA–MVs group retained the largest number of neurons, confirmed that it had the best recovery effect. To evaluate the safety of the NAL–SA–MVs, HE staining (Fig. 8) was performed on the main organs and tissues (heart, liver, spleen, lung and kidney). There were no significant pathological changes, showing that the NAL–SA–MVs had good biosafety.

## 4. Conclusion

In this experiment, NAL–SA–MVs were designed to promote functional recovery after SCI in mice. Small animal live imaging assays demonstrated the positive targeting of the

NAL–SA–MVs. *In vitro* cellular and animal experiments demonstrated that NAL–SA–MVs reduced the free $Ca^{2+}$ concentration and led to inflammation inhibition and neuroprotection. It could also significantly promote motor function recovery of the SCI mice. Therefore, NAL–SA–MVs was a promising drug delivery systems for SCI.

## Conflicts of interest

The authors declare no competing financial interest. The manuscript was written through contributions of all authors. All authors have given approval to the final version of the manuscript.

## Acknowledgment

The author(s) disclosed receipt of the following financial support for the research, authorship, and/or publication of this article: The authors acknowledge the financial support received from the Natural Science Foundation of Liaoning Province [No. 20180550155, 2021-MS-332], the National Natural Science Foundation of China (No. 81671907, 81871556, 82072165), LiaoNing Revitalization Talents Program (No. XLYC1902108), Scientific Research Project of the Educational Department of Liaoning Province (No. JYTQN201917, JYTQN201919), Liaoning Provincial Key Laboratory of Marine Bioactive Substances and Technological Innovation Center of Liaoning Pharmaceutical Action and Quality Evaluation (No. 2020–10).

## Supplementary materials

Supplementary material associated with this article can be found, in the online version, at doi:10.1016/j.ajps.2021.11.001.

REFERENCE

[1] Lin Y, Wan Y, Du X, Li J, Wei J, Li T, et al. TAT-modified serum albumin nanoparticles for sustained-release of tetramethylpyrazine and improved targeting to spinal cord injury. J Nanobiotechnol 2021;19(1):28.
[2] Selvarajah S, Hammond ER, Haider AH, Abularrage CJ, Becker D, Dhiman N, et al. The burden of acute traumatic spinal cord injury among adults in the united states: an update. J Neurotrauma 2014;31(3):228–38 Feb 1.
[3] Toluse AM, Adeyemi TO. Epidemiology and clinical outcomes of spinal cord injuries at a level II trauma centre in Nigeria: a longitudinal five year study. Int Orthop 2021;45(3):665–71.
[4] Ahuja CS, Wilson JR, Nori S, Kotter MRN, Druschel C, Curt A, et al. Traumatic spinal cord injury. Nat Rev Dis Prim 2017;3:17018.
[5] Wang XJ, Shu GF, Xu XL, Peng CH, Lu CY, Cheng XY, et al. Combinational protective therapy for spinal cord injury medicated by sialic acid-driven and polyethylene glycol based micelles. Biomaterials 2019;217:119326.
[6] Park K, Lee Y, Park S, Lee S, Hong Y, Kil LS, et al. Synergistic effect of melatonin on exercise-induced neuronal reconstruction and functional recovery in a spinal cord injury animal model. J Pineal Res 2010;48(3):270–81.
[7] Hu R, Duan B, Wang D, Yu Y, Li W, Luo H, et al. Role of acid-sensing ion channel 1a in the secondary damage of traumatic spinal cord injury. Ann Surg 2011;254(2):353–62.
[8] Ren H, Chen X, Tian M, Zhou J, Ouyang H, Zhang Z. Regulation of inflammatory cytokines for spinal cord injury repair through local delivery of therapeutic agents. Adv Sci 2018;5(11):1800529 (Weinh).
[9] Ahuja CS, Mothe A, Khazaei M, Badhiwala JH, Gilbert EA, van der Kooy D, et al. The leading edge: emerging neuroprotective and neuroregenerative cell-based therapies for spinal cord injury. Stem Cells Transl Med 2020;9(12):1509–30.
[10] Li L, Zhang Y, Mu J, Chen J, Zhang C, Cao H, et al. Transplantation of human mesenchymal stem-cell-derived exosomes immobilized in an adhesive hydrogel for effective treatment of spinal cord injury. Nano Lett 2020;20(6):4298–305 Jun 10.
[11] Guo S, Perets N, Betzer O, Ben-Shaul S, Sheinin A, Michaelevski I, et al. Intranasal delivery of mesenchymal stem cell derived exosomes loaded with phosphatase and tensin homolog siRNA repairs complete spinal cord injury. ACS Nano 2019;13(9):10015–28.
[12] Wang Q, Zhang H, Xu H, Zhao Y, Li Z, Li J, et al. Novel multi-drug delivery hydrogel using scar-homing liposomes improves spinal cord injury repair. Theranostics 2018;8(16):4429–46.
[13] Ren H, Han M, Zhou J, Zheng ZF, Lu P, Wang JJ, et al. Repair of spinal cord injury by inhibition of astrocyte growth and inflammatory factor synthesis through local delivery of flavopiridol in PLGA nanoparticles. Biomaterials 2014;35(24):6585–94.
[14] Wang XJ, Peng CH, Zhang S, Xu XL, Shu GF, Qi J, et al. Polysialic-acid-based micelles promote neural regeneration in spinal cord injury therapy. Nano Lett 2019;19(2):829–38.
[15] Song YH, Agrawal NK, Griffin JM, Schmidt CE. Recent advances in nanotherapeutic strategies for spinal cord injury repair. Adv Drug Deliv Rev 2019;148:38–59.
[16] Dong X, Gao J, Zhang CY, Hayworth C, Frank M, Wang Z. Neutrophil membrane-derived nanovesicles alleviate inflammation to protect mouse brain injury from ischemic stroke. ACS Nano 2019;13(2):1272–83.
[17] Lv W, Xu J, Wang X, Li X, Xu Q, Xin H. Bioengineered boronic ester modified dextran polymer nanoparticles as reactive oxygen species responsive nanocarrier for ischemic stroke treatment. ACS Nano 2018;12(6):5417–26.
[18] Li M, Liu Y, Chen J, Liu T, Gu Z, Zhang J, et al. Platelet bio-nanobubbles as microvascular recanalization nanoformulation for acute ischemic stroke lesion theranostics. Theranostics 2018;8(18):4870–83.
[19] Xia N, Gao Z, Hu H, Li D, Zhang C, Mei X, et al. Nerve growth factor loaded macrophage-derived nanovesicles for inhibiting neuronal apoptosis after spinal cord injury. J Biomater Appl 2021;36(2):276–88.
[20] Scholpa NE, Schnellmann RG. Mitochondrial-Based Therapeutics for the treatment of spinal cord injury: mitochondrial biogenesis as a potential pharmacological target. J Pharmacol Exp Ther 2021;201763(3):303–13.
[21] Benedict AL, Mountney A, Hurtado A, Bryan KE, Schnaar RL, Dinkova-Kostova AT, et al. Neuroprotective effects of sulforaphane after contusive spinal cord injury. J Neurotrauma 2012;29(16):2576–86.
[22] Simmons EC, Scholpa NE, Cleveland KH. Schnellmann RG. 5-hydroxytryptamine 1F receptor agonist induces mitochondrial biogenesis and promotes recovery from spinal cord injury. J Pharmacol Exp Ther 2020;372(2):216–23.

[23] Berardi A, Bauhuber S, Sawafta O, Warnke G. Alginates as tablet disintegrants: understanding disintegration mechanisms and defining ranges of applications. Int J Pharm 2021;601:120512.
[24] Liu C, Shi Z, Sun H, Mujuni CJ, Zhao L, Wang X, et al. Preparation and characterization of tissue-factor-loaded alginate: toward a bioactive hemostatic material. Carbohydr Polym 2020;249:116860.
[25] Javvaji V, Baradwaj AG, Payne GF, Raghavan SR. Light-activated ionic gelation of common biopolymers. Langmuir 2011;27(20):12591–6.
[26] Alarfaj NA, El-Tohamy MF. A high throughput gold nanoparticles chemiluminescence detection of opioid receptor antagonist naloxone hydrochloride. Chem Cent J 2015;9:6.
[27] Faden AI, Jacobs TP, Holaday JW. Opiate antagonist improves neurologic recovery after spinal injury. Science 1981;211(4481):493–4.
[28] Faden AI, Jacobs TP, Mougey E, Holaday JW. Endorphins in experimental spinal injury: therapeutic effect of naloxone. Ann Neurol 1981;10(4):326–32.
[29] Faden AI, Molineaux CJ, Rosenberger JG, Jacobs TP, Cox BM. Endogenous opioid immunoreactivity in rat spinal cord following traumatic injury. Ann Neurol 1985;17(4):386–90.
[30] Faden AI, Jacobs TP, Holaday JW. Comparison of early and late naloxone treatment in experimental spinal injury. Neurology 1982;32(6):677–81.
[31] Liu B, Du L, Kong LY, Hudson PM, Wilson BC, Chang RC, et al. Reduction by naloxone of lipopolysaccharide-induced neurotoxicity in mouse cortical neuron-glia co-cultures. Neuroscience 2000;97(4):749–56.
[32] Yacoub A, Hajec MC, Stanger R, Wan W, Young H, Mathern BE. Neuroprotective effects of perflurocarbon (oxycyte) after contusive spinal cord injury. J Neurotrauma 2014;31(3):256–67.
[33] Yang X, Chen S, Shao Z, Li Y, Wu H, Li X, et al. Apolipoprotein E deficiency exacerbates spinal cord injury in mice: inflammatory response and oxidative stress mediated by NF-$\kappa$B signaling pathway. Front Cell Neurosci 2018;12:142.
[34] Zhou K, Zheng Z, Li Y, Han W, Zhang J, Mao Y, et al. TFE3, a potential therapeutic target for spinal cord injury via augmenting autophagy flux and alleviating ER stress. Theranostics 2020;10(20):9280–302.
[35] Liu H, Zhang J, Xu X, Lu S, Yang D, Xie C, et al. SARM1 promotes neuroinflammation and inhibits neural regeneration after spinal cord injury through NF-$\kappa$B signaling. Theranostics 2021;11(9):4187–206.
[36] Moody OA, Zhang ER, Arora V, Kato R, Cotten JF, Solt K. D-amphetamine accelerates recovery of consciousness and respiratory drive after high-dose fentanyl in rats. Front Pharmacol 2020;11:585356.
[37] Liu D, Chen J, Jiang T, Li W, Huang Y, Lu X, et al. Biodegradable spheres protect traumatically injured spinal cord by alleviating the gGlutamate-induced excitotoxicity. Adv Mater 2018;30(14):e1706032.
[38] McKay CA, Pomrenke RD, McLane JS, Schaub NJ, DeSimone EK, Ligon LA, et al. An injectable, calcium responsive composite hydrogel for the treatment of acute spinal cord injury. ACS Appl Mater Interfaces 2014;6(3):1424–38.
[39] Adalbert R, Engelhardt JI, Siklós L. DL-Homocysteic acid application disrupts calcium homeostasis and induces degeneration of spinal motor neurons *in vivo*. Acta Neuropathol 2002;103(5):428–36.
[40] Xi K, Gu Y, Tang J, Chen H, Xu Y, Wu L, et al. Microenvironment-responsive immunoregulatory electrospun fibers for promoting nerve function recovery. Nat Commun 2020;11(1):4504.
[41] Vismara I, Papa S, Veneruso V, Mauri E, Mariani A, De Paola M, et al. Selective modulation of A1 astrocytes by drug-loaded nano-structured gel in spinal cord injury. ACS Nano 2020;14(1):360–71.
[42] Beck KD, Nguyen HX, Galvan MD, Salazar DL, Woodruff TM, Anderson AJ. Quantitative analysis of cellular inflammation after traumatic spinal cord injury: evidence for a multiphasic inflammatory response in the acute to chronic environment. Brain 2010;133(Pt 2):433–47.
[43] Zhang M, Xu C, Liu D, Han MK, Wang L, Merlin D. Oral delivery of nanoparticles loaded with ginger active compound, 6-shogaol, attenuates ulcerative colitis and promotes wound healing in a murine model of ulcerative colitis. J Crohns Colitis 2018;12(2):217–29.
[44] Zhang T, Tang M, Kong L, Li H, Zhang T, Xue Y, et al. Surface modification of multiwall carbon nanotubes determines the pro-inflammatory outcome in macrophage. J Hazard Mater 2015;284:73–82.
[45] Choi HJ, Choi S, Kim JG, Song MH, Shim KS, Lim YM, et al. Enhanced tendon restoration effects of anti-inflammatory, lactoferrin-immobilized, heparin-polymeric nanoparticles in an Achilles tendinitis rat model. Carbohydr Polym 2020;241:116284.
[46] Casha S, Zygun D, McGowan MD, Bains I, Yong VW, Hurlbert RJ. Results of a phase II placebo-controlled randomized trial of minocycline in acute spinal cord injury. Brain 2012;135(Pt 4):1224–36.
[47] Yu WR, Fehlings MG. Fas/FasL-mediated apoptosis and inflammation are key features of acute human spinal cord injury: implications for translational, clinical application. Acta Neuropathol 2011;122(6):747–61.
[48] Zhang B, Fan Y, Cao P, Tan K. Multifaceted roles of HSF1 in cell death: a state-of-the-art review. Biochim Biophys Acta Rev Cancer 2021;1876(2):188591 Jul 14.
[49] Chueh WH, Lin JY. Berberine, an isoquinoline alkaloid, inhibits streptozotocin-induced apoptosis in mouse pancreatic islets through down-regulating Bax/Bcl-2 gene expression ratio. Food Chem 2012;132(1):252–60.
[50] O'Neill KL, Huang K, Zhang J, Chen Y, Luo X. Inactivation of prosurvival Bcl-2 proteins activates Bax/Bak through the outer mitochondrial membrane. Genes Dev 2016;30(8):973–88.
[51] Qi G, Sun D, Tian Y, Xu C, Zhang Y, Wang D, et al. Fast activation and tracing of caspase-3 involved cell apoptosis by combined electrostimulation and smart signal-amplified SERS nanoprobes. Anal Chem 2020;92(11):7861–8.